

1 **Modulation of the Indian Monsoon by Cross-Equatorial Ocean Heat**

2 **Transport**

3 Nicholas J. Lutsko\*

4 *Department of Earth, Atmospheric, and Planetary Sciences, Massachusetts Institute of*  
5 *Technology, Cambridge, Massachusetts*

6 John Marshall

7 *Department of Earth, Atmospheric, and Planetary Sciences, Massachusetts Institute of*  
8 *Technology, Cambridge, Massachusetts*

9 Brian Green

10 *Department of Earth, Atmospheric, and Planetary Sciences, Massachusetts Institute of*  
11 *Technology, Cambridge, Massachusetts*

12 \**Corresponding author address:* Nicholas Lutsko, Department of Earth, Atmospheric, and Plane-  
13 tary Sciences, Massachusetts Institute of Technology, Cambridge, Massachusetts

14 E-mail: lutsko@mit.edu

## ABSTRACT

15 The role of the ocean circulation in modulating the Indian Monsoon is ex-  
16 plored in an idealized study in which an atmospheric model is coupled to a  
17 slab ocean with an interactive representation of ocean heat transport (OHT).  
18 Summertime southwards ocean heat transport in the cross-equatorial cells of  
19 the northern Indian Ocean (NIO) is found to play a critical role in increasing  
20 the reversed meridional surface gradient of moist static energy, shifting the  
21 precipitation maximum over land. This OHT is caused by Ekman flow driven  
22 by the southwesterly monsoon winds, and results in cooling of sea-surface  
23 temperatures (SSTs) of the NIO. The magnitude of the OHT can be systemat-  
24 ically varied in the model, allowing the influence of OHT on the monsoon to  
25 be studied. “Land” is added through use of a much reduced mixed-layer depth,  
26 and hence heat capacity. It is found that OHT strengthens the monsoon, by en-  
27 hancing the vertical wind shear and the precipitation over the land. However,  
28 at the same time, the cross-equatorial mean meridional overturning circula-  
29 tion is weakened, since less energy needs to be transported across the equator  
30 by the atmosphere. The sensitivity of these effects to fixing the OHT at its  
31 annual-mean value and to removing the land are also explored. A comparison  
32 with observations suggests that the model produces a reasonable representa-  
33 tion of the effects of OHT on the SSTs south of the continent, and if anything  
34 underestimates the effects of OHT.

## 35 **1. Introduction**

36 It is now well understood that the South Asian Monsoon is a thermally-direct circulation driven  
37 by the thermodynamic contrast which develops in the summer months between the Indian subcon-  
38 tinent and the Indian Ocean to the south (e.g., Plumb and Hou (1992); Privé and Plumb (2007a);  
39 Privé and Plumb (2007b); Bordoni and Schneider (2008); Zhai and Boos (2015); Geen et al.  
40 (2018)). Intuitively, this contrast arises because the land’s smaller heat capacity causes it to warm  
41 up faster in the summer than the surrounding waters, but recent work has shown that a number of  
42 other factors are required to maintain the gradient. Most importantly, the Himalayas play a crucial  
43 role by insulating the Indian subcontinent from cold northerly winds blowing down from central  
44 Eurasia, keeping the surface temperatures high there during summer (see Boos and Kuang (2010)  
45 and Ma et al. (2014)).

46 The other side of the contrast – the relatively cool waters of the northern Indian Ocean (NIO) –  
47 has been less explored. Privé and Plumb (2007b) compared the monsoons in simulations with their  
48 idealized atmospheric model forced by uniformly warm sea surface temperatures (SSTs) and by  
49 an SST profile that has a meridional gradient, and found that a meridional SST gradient promotes a  
50 cross-equatorial monsoon circulation. This picture was complicated, however, because the land in  
51 their idealized set-up is cooled by zonal winds coming from the colder waters adjacent to the land,  
52 damping the thermal contrast and hence the monsoon circulation (see also Chou et al. (2001)).  
53 Privé and Plumb were able to strengthen the monsoon in their model by adding “walls” around the  
54 continent to insulate it from these sea-breezes.

55 While this provided a first indication of the relationship between the NIO and the monsoon cir-  
56 culation, it was highly idealized and did not consider feedbacks between the monsoonal winds and  
57 the SSTs. Webster and co-authors have suggested that the monsoon acts as a self-regulating sys-

58 tem (Loschnigg and Webster (2000); Webster et al. (2002); Chirokova and Webster (2006)), with  
59 strong monsoonal winds driving southward ocean heat transport (OHT) in the NIO, cooling the  
60 waters adjacent to the Indian subcontinent and hence damping the monsoon. This can be seen in  
61 observations, as the surface winds are southwesterly over the NIO in the summer and southeasterly  
62 south of the equator (arrows in Figure 1). The circulation pattern drives southward Ekman flow in  
63 the NIO's mixed-layer, transporting heat into the southern hemisphere and potentially cooling the  
64 SSTs of the NIO. The heat transport can be inferred from the contours in Figure 1, which show  
65 the flux of heat from the atmosphere into the ocean. Developing a better understanding of the  
66 connection between OHT and the monsoon is the primary aim of this study.

67 The role of the Indian Ocean in cross-equatorial heat transport, but perhaps not monsoon dy-  
68 namics, has been appreciated as far back as at least Levitus (1987). He hypothesized that the  
69 Ekman response to near surface equatorial winds in the Indian Ocean resulted in southward cross-  
70 equatorial heat transport in the boreal summer, which reversed in the winter. Ideas that describe  
71 the dynamical process involved, those of the Cross Equatorial Cell, are developed in McCreary  
72 et al. (1993), whose model was adapted by Loschnigg and Webster (2000) and Chirokova and  
73 Webster (2006).

74 Separate from the question of monsoons, the relationship between the zonal-mean atmospheric  
75 circulation and OHT has been investigated in a number of recent studies. It has been shown that  
76 including interactive OHT in idealized models substantially damps the Hadley circulation (Levine  
77 and Schneider (2011); Singh et al. (2017)), as well as meridional shifts of the intertropical con-  
78 vergence zone (ITCZ, Green and Marshall (2017); Schneider (2017)). The reason for this is that,  
79 because the weak Coriolis force at low latitudes means that large temperature gradients cannot  
80 be maintained away from the surface (Sobel et al. 2001), the tropical atmosphere is an inefficient  
81 transporter of energy. By contrast, the wind-driven subtropical cells in the ocean efficiently trans-

82 port energy away from the equator because of the large surface temperature difference between  
83 the tropics and subtropics, which is mapped onto the vertical via subduction (Held (2001); Czaja  
84 and Marshall (2005); Green and Marshall (2017)). Hence including interactive OHT means that  
85 much less energy needs to be transported to high latitudes by the atmosphere. These studies have  
86 focused on the zonal-mean perspective, but similar considerations would be expected to apply to  
87 zonally-localized perturbations, such as monsoons, with the caveat that we do not yet have a good  
88 understanding of what controls the partitioning between zonal and meridional energy transports.

89 Putting these results together, coupling to the ocean has a number of competing effects on the  
90 monsoonal circulation, potentially strengthening it by enhancing the land-sea temperature gradi-  
91 ent and weakening it by cooling the waters adjacent to the land and by reducing the energetic  
92 requirements on the cross-equatorial circulation. In this study we aim to untangle these effects by  
93 investigating how the monsoon in a moist, gray radiation atmospheric general circulation model  
94 (GCM) is affected by coupling the GCM to a slab ocean with an interactive representation of OHT.  
95 The parameterization includes an ocean stratification parameter that can be varied to directly con-  
96 trol the strength of the OHT, allowing us to systematically investigate the influence of OHT on the  
97 monsoon. We have also performed sensitivity experiments without land and with the OHT fixed at  
98 its annual-mean value to separate zonally-asymmetric effects from zonal-mean effects and to cut  
99 the coupling between OHT and the monsoonal circulation.

100 We note that our focus is primarily on the seasonal-mean monsoon and not on its variability.  
101 Work with observations and comprehensive models has demonstrated a strong link between the  
102 variability of the monsoon and SSTs in the Bay of Bengal; for instance, colder SSTs in the Bay  
103 of Bengal precede monsoon “breaks”, periods when the rains are muted, by about a week (e.g.,  
104 Vecchi and Harrison (2002); Schott et al. (2009)). However this variability is unlikely to be well  
105 represented in our model because of the idealized geometries we use and also because the GCM

106 does not include a representation of clouds. As such our focus is on the mean state of the monsoon,  
 107 which our model can be expected to represent, and on the more general question of the relationship  
 108 between the zonally-asymmetric atmospheric circulation and OHT.

109 The model and the simulations we have performed are described in more detail in the next  
 110 section. In section 3 we investigate how the monsoon in our model is affected by coupling with  
 111 the OHT, including how it is affected by varying the strength of the OHT and by fixing the OHT  
 112 at its annual-mean value. In section 4 we compare the model with observations to assess how  
 113 relevant our results may be for the real South Asian Monsoon and in section 5 we present the  
 114 results of the experiments without land. We end with conclusions in section 6.

## 115 **2. Model Description and Simulations**

116 The model consists of the idealized moist GCM first described by Frierson et al. (2006), coupled  
 117 to a slab ocean with an idealized representation of OHT by the subtropical cells.

### 118 *a. The Moist GCM*

119 The GCM solves the primitive equations on the sphere and is forced by gray radiation. The long-  
 120 wave optical depth is specified to approximate the effects of atmospheric water vapor (Frierson  
 121 et al. 2006):

$$\tau(p, \phi) = \tau_0 \left[ f_l \left( \frac{p}{p_s} \right) + (1 - f_l) \left( \frac{p}{p_s} \right)^4 \right], \quad (1)$$

122 where  $p$  is pressure,  $\phi$  is latitude,  $p_s$  is the surface pressure and the linear term is included to  
 123 reduce stratospheric relaxation times ( $f_l$  is set to 0.1).  $\tau_0$  is the optical depth at the surface, and  
 124 takes the form

$$\tau_0(\phi) = \tau_{0e} + (\tau_{0p} - \tau_{0e}) \sin^2 \phi, \quad (2)$$

125 with  $\tau_{0e}$  the surface value at the equator and  $\tau_{0p}$  the surface value at the pole. These are set to 7.2  
 126 and 1.8, respectively (O’Gorman and Schneider 2008). The solar insolation has an annual cycle,  
 127 but no diurnal cycle, and is calculated as (see chapter 2 of Hartmann (2016)):

$$S_0 = \frac{S_c}{\pi} [h_0 \sin\phi \sin\delta + \cos\phi \cos\delta \sin h_0], \quad (3)$$

128 where the solar constant  $S_c$  is set to  $1360 \text{Wm}^{-2}$ ;  $h_0$  is the longitude of the subsolar point at sunrise  
 129 and sunset relative to its position at noon; and  $\delta$  is the declination, calculated using an obliquity  
 130 of  $23.45^\circ$ , a 360 day year and assuming that Earth’s orbit is perfectly circular. The albedo is fixed  
 131 at 0.38 and the absorption of solar radiation by the atmosphere is modelled by calculating the  
 132 downward shortwave flux at a given pressure level as  $S = S_0 \exp(-\tau_s (p/p_s)^2)$ , with  $\tau_s$  fixed at  
 133 0.22, as used by O’Gorman and Schneider (2008).

134 The model includes the simplified Betts-Miller (SBM) convection scheme of Frierson (2007),  
 135 with a convective relaxation time-scale  $\tau_{\text{SBM}}$  of 2 hours and a reference relative humidity  $RH_{\text{SBM}}$   
 136 = 0.7, and the boundary layer scheme is the one used by O’Gorman and Schneider (2008). In  
 137 each experiment the model was integrated for four years at T85 truncation (corresponding to a  
 138 resolution of roughly  $1.4^\circ$  by  $1.4^\circ$  on a Gaussian grid) with 30 vertical levels extending up to  
 139 16hPa. Averages were taken over the last three years of each simulation.

#### 140 *b. Interactive OHT parameterization*

141 OHT can be represented as the product of a meridional overturning circulation and an energy  
 142 contrast (Held (2001); Czaja and Marshall (2005))

$$q_O = c_{p,o} \Phi \Delta T, \quad (4)$$

143 where  $c_{p,o}$  is the heat capacity of seawater,  $\Phi$  is the overturning mass transport streamfunction  
 144 and  $\Delta T$  is the temperature difference across the upper and lower branches of the overturning cir-

145 culation, i.e., between the top and base of the subtropical cells. This can also be thought of as  
 146 the surface temperature difference between the deep tropics and the latitude of subduction, with  
 147 typical values of 5-10K (Klinger and Marotzke 2000).

148 In the tropics, the oceanic mass transport is mostly set by the Ekman mass transport, allowing  
 149 us to approximate the OHT as

$$q_O(\phi, \lambda) \approx a c_{p,o} \cos\phi \frac{\tau(\phi, \lambda)}{f(\phi)} \Delta T, \quad (5)$$

150 where  $\lambda$  is longitude,  $a$  is the radius of the Earth,  $\tau$  is the wind stress and  $f$  is the Coriolis paramete-  
 151 ter. The interactive OHT parameterization assumes that heat is only transported via equation 5, and  
 152 only calculates the OHT for latitudes between  $\phi_1$ , the latitude at which the surface winds change  
 153 from westerly to easterly in the southern hemisphere, and  $\phi_2$ , the latitude at which the surface  
 154 winds change from easterly to westerly in the northern hemisphere.  $c_{p,o}$  is set to  $3900 \text{ Jkg}^{-1} \text{ K}^{-1}$   
 155 and, importantly,  $\Delta T$  is left as a free parameter to be specified.

156 This parameterization is similar to the scheme used by Klinger and Marotzke (2000) and Levine  
 157 and Schneider (2011), except that their scheme uses surface quantities, so that the OHT is calcu-  
 158 lated from the surface wind and temperature fields, with no free parameters. Here we specify  $\Delta T$   
 159 directly in order to systematically investigate how the strength of the OHT impacts the monsoon,  
 160 as larger  $\Delta T$  values result in more heat being transported southwards in the summer. Our scheme is  
 161 also similar to the “1.5-layer” parameterization of Ekman heat transport by Codron (2012), though  
 162 we have excluded diffusive heat transport and only focus on heat transport in the tropics.

163 As in Levine and Schneider (2011), we apply a Gaussian smoothing filter when calculating the  
 164 divergence of the heat flux to avoid issues with  $f$  going to zero at the equator:

$$(\nabla \cdot q_O)' = \int_{\phi_1}^{\phi_2} \frac{1}{a \cos\phi} (\nabla \cdot q_O) P(\phi, \phi') d\phi', \quad (6)$$

165 where

$$P(\phi, \phi') = \frac{1}{Z} \exp\left(\frac{-(\phi' - \phi)^2}{2s^2}\right), \quad (7)$$

166 with  $Z$  chosen such that the integral of  $P$  from  $\phi_1$  to  $\phi_2$  is equal to one and  $s$  a half-width, which is  
167 set to  $7^\circ$ .

168 The depth of the ocean is fixed at 24m in all of our simulations. Donohoe et al. (2014) found  
169 that coupling the CM2.1 GCM to a 24m slab ocean produced a climate with a reasonable seasonal  
170 migration of the ITCZ compared with observations, and also a reasonable annual-mean Hadley  
171 circulation and meridional distribution of precipitation.

172 “Land” is added to the model by reducing the mixed-layer depth to 0.5m and setting the ocean  
173 heat flux divergence to zero between  $100^\circ - 235^\circ\text{E}$  and  $15^\circ - 40^\circ\text{N}$ . This provides an infinite  
174 supply of moisture for the monsoonal circulation and also means that the global integral of  $q_0$   
175 is not always zero. So there may be net OHT from the northern hemisphere into the southern  
176 hemisphere, even for conditions that are otherwise hemispherically-symmetric, however we find  
177 that in the annual-mean the ITCZ is very close to the equator in all of our simulations (not shown).  
178 The geometry of our set-up is illustrated in Figure 2.

### 179 *c. Simulations*

180 We have performed three sets of simulations with the model, motivated by our aim of untangling  
181 the competing effects of OHT on the monsoon. The main set includes both land and the interactive  
182 OHT, with  $\Delta T$  varied from 0K (i.e., no OHT) to 15K. In a second set of simulations the OHT at  
183 each grid point is fixed at its annual-mean value from the first set of simulations, eliminating the  
184 coupling between OHT and the monsoonal circulation but maintaining the annual-mean effects of  
185 OHT. The third set include the interactive OHT but not the land, with  $\Delta T$  again varied from 0K to

186 15K. Comparing these simulations with the first set of simulations allows the impacts of the OHT  
187 on the zonal-mean circulation to be separated out.

### 188 **3. The Relationship Between OHT and the Model’s Monsoon**

#### 189 *a. Comparing Simulations With and Without OHT*

190 We begin by comparing the monsoons in a simulation without OHT and a simulation with  $\Delta T$   
191 = 10K, which is one of our more realistic simulations (see section 4). Figure 3 shows the sum-  
192 mertime<sup>1</sup> precipitation and surface winds (top panels), the summertime surface moist static energy  
193 (middle panels) and the summertime ocean heat flux divergence for the interactive case (bottom  
194 right panel). The surface moist static energy is calculated as  $c_p T + L_v q_v$ , where  $c_p$  is the specific  
195 heat capacity of dry air,  $T$  is the temperature at the lowest model level,  $L_v$  is the latent heat of  
196 vaporization of liquid water and  $q_v$  is the specific humidity at the lowest model level.

197 Without OHT, the ITCZ is slightly north of the equator, at about 5°N in the zonal-mean, and  
198 there is also a weak precipitation maximum just south of the continent. The surface MSE is  
199 relatively uniform throughout the tropics, though the largest values are on the southern edge of the  
200 continent so that the highest precipitation in the land sector is substantially further equatorward of  
201 the MSE maximum. The winds resemble the observations (Figure 1), being southeasterly up to  
202 about 5°N and then swinging around to be southwesterly between 5°N and 20°N, but the winds  
203 north of 5° are weak.

204 In the simulation with OHT there is much clearer evidence of a monsoon, with the highest  
205 precipitation over the southern edge of the continent, at about 17°N. The winds again resemble  
206 the observations, and are stronger between 5°N and 20°N than in the no OHT case. The surface  
207 MSE is generally smaller than in the simulation without OHT, because the OHT parameterization

---

<sup>1</sup>In the simulations we define “summer” as the 90 warmest days over the land and “winter” as the 90 coldest days over the land.

208 redistributes heat to the subtropics, and there is a sharper maximum in MSE over the continent,  
209 resulting in a larger land-ocean contrast in low-level MSE. Panel e) of Figure 3 shows that the  
210 ocean transports heat southwards across the equator, as well as from the tropics into the subtropics  
211 of the Northern Hemisphere.

212 Figure 4 compares the seasonal cycles in precipitation (top panels) and surface MSE (bottom  
213 panels) in these simulations, with values averaged over the land sector. Without OHT the maxi-  
214 mum precipitation varies smoothly over the course of the year, following the maximum insolation,  
215 though there is increased precipitation just south of the land in the late spring and summer months.  
216 The MSE shows a similar progression, and the largest MSE is in the summer and early fall because  
217 of the larger warming of the land.

218 The seasonal cycle of precipitation is less regular when OHT is included, and the maximum pre-  
219 cipitation is weaker than in the simulation without OHT (panel c). Both the precipitation and the  
220 maximum MSE jump to the warmer hemisphere during the transition seasons. The amplitude of  
221 the seasonal cycle in MSE is larger in the Northern Hemisphere than in the Southern Hemisphere,  
222 as the highest MSE values are found over the land in the summer months, while the lowest MSE  
223 values are over the land in the winter months. This is discussed further in section 5.

#### 224 *b. Varying $\Delta T$*

225 The effects of varying the strength of the OHT on the surface climate of the model are summa-  
226 rized in Figure 5. As  $\Delta T$  is increased the tropical SSTs in the land sector cool and the meridional  
227 SST gradient is reduced (panel a). However the land-ocean surface temperature contrast increases  
228 dramatically, going from about 0.2K to 1.5K as  $\Delta T$  is increased from 0K to 15K. The MSE has  
229 a similar progression (panel b), though the profile is smoother, without such a sharp jump across  
230 the land-ocean boundary, because of the specific humidity (panel d). A secondary MSE maximum

231 develops in the southern hemispheres of the experiments with large  $\Delta T$ , due to a maximum in the  
232 specific humidity.

233 The ITCZ is close to  $5^\circ\text{N}$  in the 0K and 2.5K simulations, before jumping over the land in the  
234 5K simulation. This appears to be an intermediate case, as the ITCZs in the 10K and 15K are very  
235 similar to each other. The OHT is also similar in these two simulations (panel e), suggesting that  
236 it may saturate for large enough  $\Delta T$ . Privé and Plumb (2007a) showed that precipitation maxima  
237 will occur slightly equatorward of maxima in the surface MSE, where the meridional gradient in  
238 surface MSE (to which the vertical wind shear is proportional) is largest. Although the maximum  
239 MSE in the 0K and 2.5K cases is over the land, there are also MSE maxima near  $5^\circ\text{N}$  in these  
240 simulations.

241 Figure 6 plots the zonal-winds in these simulations in black contours and the mean meridional  
242 circulation (MMC) in the red contours. The MMC is calculated as  $\frac{1}{g} \int_{p_s}^p \bar{v}(p', \phi) dp'$ , where an  
243 overbar denotes an average over the land sector. The overturning circulation expands and weakens  
244 as  $\Delta T$  is increased, while the vertical shear in the zonal wind, which is often taken as a proxy for the  
245 strength of the monsoonal circulation (Webster and Yang 1992), increases. This is primarily due  
246 to a strengthening of the easterlies near the tropopause. For larger  $\Delta T$  a jump in the near-surface  
247 meridional circulation develops just north of the equator because of the difficulty the return flow of  
248 the Hadley circulation has in crossing the equator close to the surface when the equatorial surface  
249 temperature gradient is weak (Pauluis 2004).

250 The round markers in Figure 7 quantify these changes by showing the maximum vertical zonal  
251 wind shear ( $u(850\text{hPa}) - u(250\text{hPa})$ ) between the equator and  $20^\circ\text{N}$  as a function of  $\Delta T$  in panel a)  
252 and the minimum (i.e., the most negative) values of the MMC as a function of  $\Delta T$  in panel b). The  
253 zonal wind shear increases slightly when going from 0K to 2.5K, then jumps at 5K and increases  
254 roughly linearly as  $\Delta T$  is increased further. Comparing with panel c) of the Figure shows that

255 this progression closely tracks the changes in the MSE gradient. In an angular momentum (AM)  
256 conserving flow the zonal-wind shear is proportional to the subcloud MSE gradient (Emanuel  
257 1995) and, though the flow in these simulations is far from the AM-conserving limit (see below),  
258 we believe that this argument is still relevant here.

259 Conversely, the strength of the MMC decreases roughly linearly from 0K to 10K and then in-  
260 creases slightly for  $\Delta T = 15\text{K}$ . The decrease over the first four simulations is expected from the  
261 discussion in the introduction: as  $\Delta T$  is increased the atmosphere has to transport less energy  
262 across the equator and so the circulation slows down. A quantitative theory for the compensation  
263 between energy transport by the Hadley circulation and OHT is still lacking, however, and in par-  
264 ticular requires a better understanding of how the gross moist stability of the tropical atmosphere  
265 is controlled (Singh et al. 2017).

266 Panel d) of Figure 7 shows the minimum absolute vorticity ( $f + \bar{\zeta}$ , where  $f$  is the Coriolis  
267 parameter and  $\zeta$  is the relative vorticity) polewards of  $7^\circ$  during the summer of these simulations.  
268 The absolute vorticity vanishes in the upper troposphere of an AM-conserving flow and, although  
269 none of the simulations are close to this regime, there is a substantial decrease in the minimum  
270 absolute vorticity, from about  $0.55 \times 10^{-5}\text{s}^{-1}$  to  $0.41 \times 10^{-5}\text{s}^{-1}$  when going from  $\Delta T = 10\text{K}$   
271 to  $\Delta T = 15\text{K}$ . This step towards an AM-conserving flow is caused by the increased vertical wind  
272 shear, as the stronger upper-level easterlies shield the tropical circulation from baroclinic eddies  
273 originating at mid-latitudes (Bordoni and Schneider 2008). Since these eddies act as a drag on  
274 the mean flow, increased shielding may explain why the MMC strengthens in the  $\Delta T = 15\text{K}$  case  
275 (Walker and Schneider 2006).

276 In summary, increasing  $\Delta T$  both strengthens the monsoonal circulation by increasing the land-  
277 sea contrast and damps the monsoon because less heat needs to be carried across the equator by  
278 the atmosphere.

279 *c. Specifying the OHT*

280 The effects of the OHT on the monsoon come partly from the seasonal variations in the OHT  
281 and partly from the effects of the annual-mean OHT. Our second set of simulations separate these  
282 out, as the OHT is fixed at the annual-mean profiles from the interactive experiments. The crosses  
283 in the top panels of Figure 7 show that this increases the maximum zonal-wind shear and also the  
284 MMC. The MSE gradient also increases (panel c), while the minimum absolute vorticity decreases  
285 rapidly, so that the flow is approximately AM-conserving for  $\Delta T = 10\text{K}$  and above (panel d).  
286 While this transition to an AM-conserving regime will strengthen the flow somewhat, panel e) of  
287 the Figure shows that in fact the MMC scales linearly with the OHT at the equator, so that the  
288 energetic requirements on the Hadley circulation are the dominant control on its strength.

289 More insight into the effects of specifying the OHT on the monsoon comes from the left panels  
290 Figure 8, which show the summer climate in the case with the OHT from the  $\Delta T = 10\text{K}$  case. The  
291 monsoon is stronger than in the corresponding case with interactive OHT, with stronger winds  
292 and precipitation, as well as a larger land-sea MSE contrast. The shape of the winds means in  
293 particular that the monsoon is strongest in the southeast corner of the continent. The reason for  
294 this stronger monsoon can be seen by comparing panel e), which shows the OHT divergence  
295 in this simulation, with panel e) of Figure 3. The annual-mean OHT is still southwards in the  
296 land sector, but the ocean now converges heat at the latitudes of the south coast of the continent  
297 ( $15\text{-}20^\circ$ ), rather than diverging heat as it was in the interactive case. This warms the waters on  
298 either side of the continent, so that the continent is not cooled as much by zonal breezes as it was  
299 in the interactive case. This is reminiscent of how Privé and Plumb (2007b) found that adding  
300 walls to their continent strengthened the monsoon by insulating it from zonal sea breezes (see  
301 Introduction).

## 302 4. Comparing with Observations

303 The above results give an indication of how interactive OHT might affect the South Asian mon-  
 304 soon, however the idealized nature of our model makes it unclear how relevant our results are for  
 305 the real atmosphere. In particular, from the point of view of simulating seasonal variability, the  
 306 main drawback of the interactive OHT parameterization is that the mixed-layer depth (MLD) is  
 307 kept fixed. In the real ocean changes in OHT do not necessarily lead to changes in SSTs, because  
 308 the MLD may also deepen or shoal.

309 The heat budget for a volume of ocean water is

$$Q_S(t) = Q_O(t) + Q_F(t), \quad (8)$$

310 where  $Q_S$  is the change in heat stored in the volume:

$$Q_S(t) = a^2 \rho c_{p,0} \int_{MLD}^0 \int_{\phi_1}^{\phi_2} \int_{\lambda_1}^{\lambda_2} \frac{dT}{dt} \cos\phi d\lambda d\phi dz, \quad (9)$$

311 with  $\rho$  the density of seawater and  $T$  is the depth-averaged temperature of the mixed-layer.  $Q_O$   
 312 is the OHT ( $q_O$ ) integrated around the lateral boundaries of the volume, as well as heat fluxed  
 313 through the bottom of the mixed-layer (which we ignore) and  $Q_F$  is the surface heat flux into the  
 314 water:

$$Q_F(t) = a^2 \int_{\phi_1}^{\phi_2} \int_{\lambda_1}^{\lambda_2} (Q_{SW} + Q_{LW} + Q_{LH} + Q_{SH}) \cos\phi d\lambda d\phi, \quad (10)$$

315 where  $Q_{SW}$  is the incoming solar radiation at the surface,  $Q_{LW}$  is the outgoing longwave radiation  
 316 at the surface,  $Q_{LH}$  is the surface latent heat flux and  $Q_{SH}$  is the surface sensible heat flux. Note  
 317 that if  $Q_F$  is fixed then changes in  $Q_O$  can be compensated either by changes in  $T$  or by changes  
 318 in the MLD and so since the MLD is fixed in our model changes in  $Q_O$  can only be compensated  
 319 by changes in  $T$ .

320 Figure 9a shows the heat budget for the ocean off the coast of the continent ( $100^\circ$  to  $235^\circ\text{E}$   
321 and  $0$  to  $15^\circ\text{N}$ ) for the simulation with land and  $\Delta T = 10\text{K}$ , which we consider to be one of our  
322 most realistic simulations. The ocean carries heat north across the equator in winter and south in  
323 summer, while it is warmed by the surface fluxes in summer and cooled in the winter. The largest  
324 surface fluxes are in the spring and in the fall because the strong monsoon winds in the summer  
325 lead to enhanced evaporative cooling over the ocean. These terms produce a seasonal cycle of  
326  $\sim 4\text{K}$  in the SSTs (solid line in Figure 9b), with the warmest SSTs in the fall when the OHT and  
327 the monsoonal winds are weaker.

328 These results agree qualitatively with previous studies of the heat budget of the NIO, though  
329 there are some notable differences. Comparing with Figure 3 of Chirokova and Webster (2006),  
330 the seasonal cycles of the OHT and of the surface fluxes in our simulations are similar to their  
331 modelled NIO, except that the OHT is generally larger than the surface fluxes in their simulations  
332 whereas the reverse is the case in our simulations (though we note that because of our idealized  
333 set-up we are not averaging over the same geometries). The other major difference is that in their  
334 simulations  $Q_F$  is almost zero during the summer and early fall, because increased cloudiness  
335 reduces the solar radiation absorbed by the surface (as a reminder, there are no clouds in our  
336 model) and because of stronger evaporative cooling than in our simulations caused by stronger  
337 monsoonal winds. The large reduction in  $Q_F$  in the summer means that the warmest SSTs in the  
338 NIO are actually in April and May (dashed line in Figure 9b), rather than in the fall.

339 Babu et al. (2004) showed that the MLD in the NIO is shallowest in February and March, which  
340 contributes to the warm SSTs in the spring, and then deepens over the course of the summer due  
341 to mixing caused by the monsoonal winds. The mixed-layer shoals rapidly again in the fall at  
342 the end of the monsoon season and then deepens in the winter months. The gradual deepening  
343 of the mixed-layer during the summer will damp the cooling of the NIO SSTs by OHT during

344 the summer months, but on the whole we believe that our model underestimates the cooling of  
345 the NIO SSTs by OHT, and the amplitude of the seasonal cycle of SSTs in the NIO is smaller  
346 than in our model (Figure 9b). So although there are differences between the heat budgets of our  
347 model and in more realistic models due to the fixed mixed-layer depth in our model and the lack  
348 of clouds, we believe that our model qualitatively captures the impact of OHT in the NIO on the  
349 SSTs south of the Indian subcontinent.

## 350 **5. Zonal-Mean Effects**

351 The behavior discussed in section 3 comes from the monsoon generated over the land, but also  
352 from the zonal-mean effects of the interactive OHT. We use our third set of experiments – with  
353 interactive OHT but no land – to investigate how the interactive OHT affects the zonal-mean  
354 circulation of the model.

355 The triangles in Figure 7a show that excluding the land reduces the vertical zonal wind shear by  
356 roughly half, though this still increases as  $\Delta T$  is increased and the MSE gradient also strengthens  
357 (panel b). So, even without the land the southward energy transport by the ocean still produces  
358 a monsoon-like circulation. The MMC is very similar with and without land (Figure 7b), as it is  
359 mostly determined by the OHT (section 3.3).

360 These experiments, together with the fixed OHT experiments, can also be used to understand the  
361 seasonal cycles in Figure 4. In the simulation without land and with  $\Delta T = 10\text{K}$  there are actually  
362 three maxima in the precipitation (Figure 10a), one close to the equator and one further polewards  
363 in each hemisphere, with all three shifting gradually over the course of the year. A double-ITCZ  
364 structure is expected because the OHT and the heat transport by the atmosphere result in the net  
365 energy input to the deep tropics being negative (Bischoff and Schneider 2016), while the peak at

366 the equator is caused by rising motion as the meridional circulation jumps over the equator (not  
367 shown).

368 The fixed OHT experiment resembles the original Hovmuller diagrams, but with the features  
369 exaggerated (Figure 10c and f). In the winter there is very little precipitation in the northern hemi-  
370 sphere and a strong maximum in precipitation at about  $-15^{\circ}\text{S}$ . A strong maximum appears in the  
371 northern hemisphere over the land in the spring, while the maximum in the southern hemisphere  
372 weakens and gradually shifts to the north, joining the strong peak over the land in the late sum-  
373 mer. During the fall the maximum slowly migrates southwards, before jumping further south once  
374 winter sets in.

375 These jumps are primarily caused by strong surface winds blowing south off the continent in the  
376 winter (Figure 8b). Because the continent is very cold in the winter, these winds cool the oceans  
377 to the south of the continent, creating a strong meridional MSE gradient compared to the warmer  
378 waters of the southern hemisphere (Figure 8d; note that the MSE near the equator is colder than  
379 in the summer). These winds die down in the spring as the land, and the oceans to either side  
380 of it, warm up, rapidly reducing the MSE gradient and causing a strong MSE and precipitation  
381 maximum to develop over the continent. At the same time, the precipitation maximum in the  
382 south migrates northwards, following the peak insolation, until it merges with the maximum over  
383 the land. In the fall the land cools and the MSE maximum gradually migrates southwards until the  
384 strong winds pick up again, rapidly cooling the ocean and causing the jump to the strong southern  
385 precipitation maximum during winter.

386 We have performed an additional experiment without land and with the OHT fixed at its annual-  
387 mean value from the no-land  $\Delta T = 10\text{K}$  experiment. This is similar to the fixed OHT with land,  
388 though the precipitation maxima are weaker (Figure 10b). The MSE is smallest in the transition  
389 months (Figure 10e), when it has a minimum near the equator because the atmosphere and ocean

390 transport heat to higher latitudes, resulting in a double-ITCZ. In the summer and winter, the atmo-  
391 sphere transfers heat into the tropics, so that they gain energy in the net (not shown) and there is a  
392 single ITCZ.

393 Together, these can explain the features seen in Figure 4. The jumps in the precipitation max-  
394 imum and in the MSE maximum come about because of the rapid warming and cooling of the  
395 continent, but at the same time the interactive OHT often results in a double ITCZ, as there is net  
396 energy transport out of the deep tropics.

## 397 **6. Conclusion**

398 In this study we have investigated the monsoon in an idealized model consisting of the widely  
399 used gray-radiation atmospheric GCM, coupled to an idealized parameterization of ocean heat  
400 transport by the subtropical cells. The OHT parameterization includes a parameter,  $\Delta T$ , which can  
401 be used to vary the strength of the OHT, allowing us to systematically investigate the impact of  
402 OHT on the monsoon in this model.

403 Without OHT the monsoon in our model is weak, because the land surface is not protected  
404 from cold winds coming either from further north or from the east and west of the land (see also  
405 Chou et al. (2001) and Privé and Plumb (2007b)). However, by increasing  $\Delta T$  sufficiently we are  
406 able to create a reasonable monsoon circulation because the waters south of the land cool during  
407 the summer, creating a strong meridional MSE gradient. This includes increases in the vertical  
408 wind shear as  $\Delta T$  is increased and in the precipitation over land, though the MMC weakens.  
409 The shear strengthens because the meridional MSE gradient increases, while the MMC weakens  
410 because the increased OHT means that the atmosphere is required to transport less heat across the  
411 equator. For  $\Delta T = 15\text{K}$  the vertical shear is strong enough to start pushing the flow towards an  
412 angular momentum-conserving regime. Fixing the OHT at its annual-mean value results in the

413 OHT warming the waters zonally-adjacent to the land, rather than cooling them, as in the case  
414 with interactive OHT, but the waters south of the land are still cooled as there is southwards OHT  
415 in the land sector (Figure 8e). This increases the MSE gradient compared to the interactive case,  
416 resulting in a stronger monsoon circulation, which causes the flow in the simulations with  $\Delta T =$   
417 10K and above to be in an AM-conserving regime. A comparison with observations and more  
418 realistic models of the Northern Indian Ocean suggests that the effects of our parameterized OHT  
419 on the SSTs south of the continent are reasonable, and if anything underestimate the effects of  
420 OHT.

421 Combining the original experiments with the fixed OHT experiments and the experiments with-  
422 out land showed that the changes in the MMC are largely due to changes in the OHT, with the  
423 MMC weakening as the OHT increased. By contrast, the presence of land and/or of a transition to  
424 an AM-conserving regime have minor impacts the MMC, except in so far as they effect the OHT.  
425 Finally, the seasonal cycle of precipitation in the interactive OHT simulations exhibits jumps, as  
426 strong precipitation suddenly appears over the continent in the summer and in the southern hemi-  
427 sphere during winter. These jumps are even clearer in the simulations with fixed OHT, and are  
428 caused by strong winds blowing off the continent during the winter months, which cool the waters  
429 south of the continent and set-up a strong MSE maximum in the southern hemisphere. When the  
430 land warms up sufficiently these winds stop and the waters north of the equator warm up quickly,  
431 while an MSE maximum develops over the land. When the land starts to cools in the fall the  
432 MSE maximum at first gradually shifts southwards, until the strong winds reappear and the max-  
433 imum MSE jumps southwards. The jumps are clearer in the simulations without the interactive  
434 OHT because removing the link between OHT and the surface winds reduces the variability of the  
435 precipitation and also makes the model less likely to have a double-ITCZ.

436 These results have been obtained with an idealized model, but demonstrate the substantial impact  
437 OHT can have on the monsoonal circulation, both through the zonal-mean effect of the atmosphere  
438 needing to transport less heat across the equator and through the local effect of creating a stronger  
439 meridional MSE gradient. Work with more realistic models, which include realistic topography, is  
440 required to fully quantify the impact these effects have on the South Asian Monsoon. Furthermore,  
441 as has been noted in several previous studies, a theory for the compensation between the ocean  
442 and the atmosphere is required in order to quantitatively predict how the overturning circulation  
443 is affected by the increased OHT, particularly a theory for how the gross moist stability of the  
444 tropical atmosphere is affected.

445 The Indian subcontinent seems to be ideally situated to develop a strong monsoon, being insu-  
446 lated from cold winds blowing down from Eurasia by the Himalayas to the north, while to the  
447 south the northern Indian Ocean transports heat southwards, cooling the SSTs off the coast of In-  
448 dia and further enhancing the meridional MSE gradient. A better understanding of the roles each  
449 of these features play in setting up the monsoon, and of how they interact with each other, will be  
450 required for a complete picture of the South Asian Monsoon.

451 *Acknowledgment.* We thank Peter Webster and Tim Cronin for helpful discussions. Nicholas  
452 Lutsko was partly supported by NSF grant AGS-1623218, “Collaborative Research: Using a Hi-  
453 erarchy of Models to Constrain the Temperature Dependence of Climate Sensitivity”.

## 454 **References**

455 Babu, K. N., R. Sharma, N. Agarwal, A. V. K., and W. R. A., 2004: Study of the mixed layer depth  
456 variations within the north indian ocean using a 1d model. *Journal of Geophysical Research:*  
457 *Oceans*, **109** (C8).

- 458 Bischoff, T., and T. Schneider, 2016: The equatorial energy balance, itcz position, and double itcz  
459 bifurcations. *Journal of Climate*, **29 (15)**, 2997–3013.
- 460 Boos, W. R., and Z. Kuang, 2010: Dominant control of the south asian monsoon by orographic  
461 insulation versus plateau heating. *Nature*, **463 (23)**, 218–222.
- 462 Bordoni, S., and T. Schneider, 2008: Monsoons as eddy-mediated regime transitions of the tropical  
463 overturning circulation. *Nature Geoscience*, **1 (23)**, 515–519.
- 464 Chirokova, G., and P. J. Webster, 2006: Interannual variability of indian ocean heat transport.  
465 *Journal of Climate*, **19 (6)**, 1013–1031.
- 466 Chou, C., J. D. Neelin, and H. Su, 2001: Ocean-atmosphere-land feedbacks in an idealized mon-  
467 soon. *Quarterly Journal of the Royal Meteorological Society*, **127 (15)**, 1869–1891.
- 468 Codron, F., 2012: Ekman heat transport for slab oceans. *Climate Dynamics*, **38 (1)**, 379–389.
- 469 Czaja, A., and J. Marshall, 2005: The partitioning of poleward heat transport between the atmo-  
470 sphere and ocean. *Journal of the Atmospheric Sciences*, **63**, 1498–1511.
- 471 Donohoe, A., D. M. W. Frierson, and D. S. Battisti, 2014: The effect of ocean mixed layer depth  
472 on climate in slab ocean aquaplanet experiments. *Climate Dynamics*, **43 (3)**, 1041–1055.
- 473 Emanuel, K. A., 1995: On thermally direct circulations in moist atmospheres. *Journal of the*  
474 *Atmospheric Sciences*, **52 (15)**, 1529–1534.
- 475 Frierson, D. M. W., 2007: The dynamics of idealized convection schemes and their effect on the  
476 zonally averaged tropical circulation. *Journal of the Atmospheric Sciences*, **64 (23)**, 1959–1976.
- 477 Frierson, D. M. W., I. M. Held, and P. Zurita-Gotor, 2006: A gray-radiation aquaplanet moist gcm.  
478 part i: Static stability and eddy scales. *Journal of the Atmospheric Sciences*, **63 (23)**, 2548–2566.

- 479 Geen, F., F. H. Lambert, and G. K. Vallis, 2018: Regime change behavior during asian monsoon  
480 onset. *Journal of Climate*, **31 (9)**, 3327–3348.
- 481 Green, B., and J. Marshall, 2017: Coupling of trade winds with ocean circulation damps itcz shift.  
482 *Journal of Climate*, **30 (12)**, 4395–4411.
- 483 Hartmann, D. L., 2016: *Global Physical Climatology*. 2nd ed., Elsevier.
- 484 Held, I. M., 2001: The partitioning of the poleward energy transport between the tropical ocean  
485 and atmosphere. *Journal of the Atmospheric Sciences*, **58**, 943–948.
- 486 Klinger, B. A., and J. Marotzke, 2000: Meridional heat transport by the subtropical cell. *Journal*  
487 *of Physical Oceanography*, **30 (23)**, 696–705.
- 488 Levine, X. J., and T. Schneider, 2011: Response of the hadley circulation to climate change in  
489 an aquaplanet gcm coupled to a simple representation of ocean heat transport. *Journal of the*  
490 *Atmospheric Sciences*, **68 (8)**, 769–783.
- 491 Levitus, S., 1987: Meridional ekman heat fluxes for the world ocean and individual ocean basins.  
492 *Journal of Physical Oceanography*, **17 (23)**, 1484–1492.
- 493 Loschnigg, J., and P. J. Webster, 2000: A coupled oceanatmosphere system of sst modulation for  
494 the indian ocean. *Journal of Climate*, **13 (104)**, 3342–3360.
- 495 Ma, D., W. R. Boos, and Z. Kuang, 2014: Effects of orography and surface heat fluxes on the  
496 south asian summer monsoon. *Journal of Climate*, **27 (9)**, 6647–6659.
- 497 McCreary, J. P., P. K. Kundu, and R. L. Molinari, 1993: A numerical investigation of the dynamics,  
498 thermodynamics and mixed layer processes in the indian ocean. *Progress in Oceanography*,  
499 **31 (23)**, 181–244.

500 O’Gorman, P. A., and T. Schneider, 2008: The hydrological cycle over a wide range of climates  
501 simulated with an idealized gcm. *Journal of Climate*, **21 (15)**, 3815–3832.

502 Pauluis, O., 2004: Boundary layer dynamics and cross-equatorial hadley circulation. *Journal of*  
503 *the Atmospheric Sciences*, **61 (23)**, 1161–1173.

504 Plumb, R. A., and A. Y. Hou, 1992: The response of a zonally symmetric atmosphere to sub-  
505 tropical thermal forcing: Threshold behavior. *Journal of the Atmospheric Sciences*, **49 (23)**,  
506 1790–1799.

507 Privé, N. C., and R. A. Plumb, 2007a: Monsoon dynamics with interactive forcing. part i: Ax-  
508 isymmetric studies. *Journal of the Atmospheric Sciences*, **64 (23)**, 1417–1430.

509 Privé, N. C., and R. A. Plumb, 2007b: Monsoon dynamics with interactive forcing. part ii: Impact  
510 of eddies and asymmetric geometries. *Journal of the Atmospheric Sciences*, **64 (23)**, 1431–1442.

511 Schneider, T., 2017: Feedback of atmosphere-ocean coupling on shifts of the intertropical conver-  
512 gence zone. *Geophysical Research Letters*, **44 (12)**, 11 644–11 653.

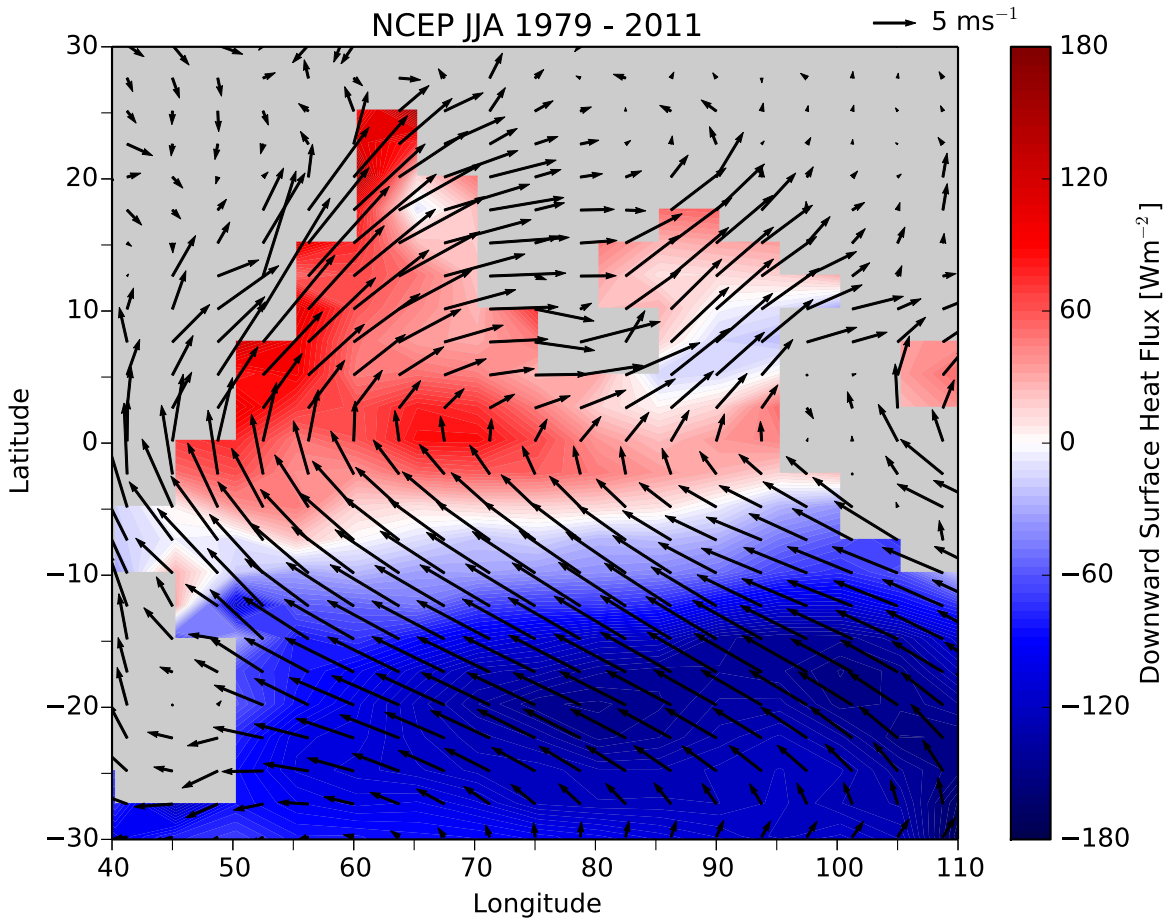
513 Schott, F. A., S.-P. Xie, and J. P. McCreary, 2009: Indian ocean circulation and climate variability.  
514 *Reviews of Geophysics*, **47 (1)**.

515 Singh, M. S., Z. Kuang, and Y. Tian, 2017: Eddy influences on the strength of the hadley circula-  
516 tion: Dynamic and thermodynamic perspectives. *Journal of the Atmospheric Sciences*, **74 (15)**,  
517 467–486.

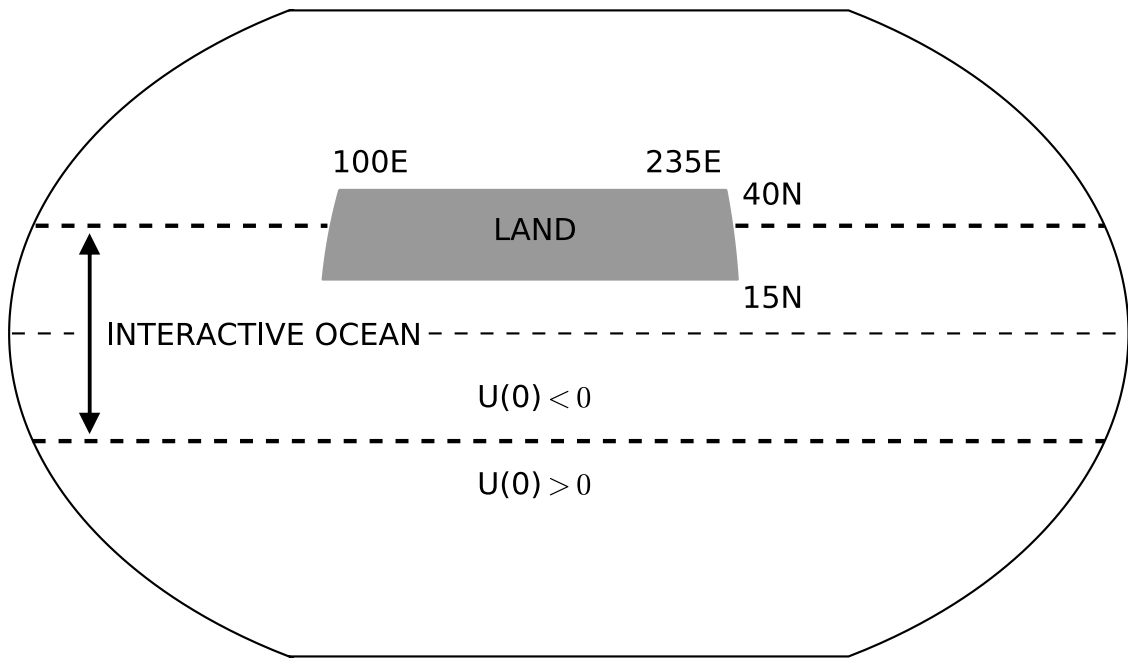
518 Sobel, A., J. Nilsson, and L. M. Polvani, 2001: The weak temperature gradient approximation and  
519 balanced tropical moisture waves. *Journal of the Atmospheric Sciences*, **58**, 3650–3665.

520 Vecchi, G. A., and D. E. Harrison, 2002: Monsoon breaks and subseasonal sea surface temperature  
521 variability in the bay of bengal. *Journal of Climate*, **15 (1)**, 1485–1493.

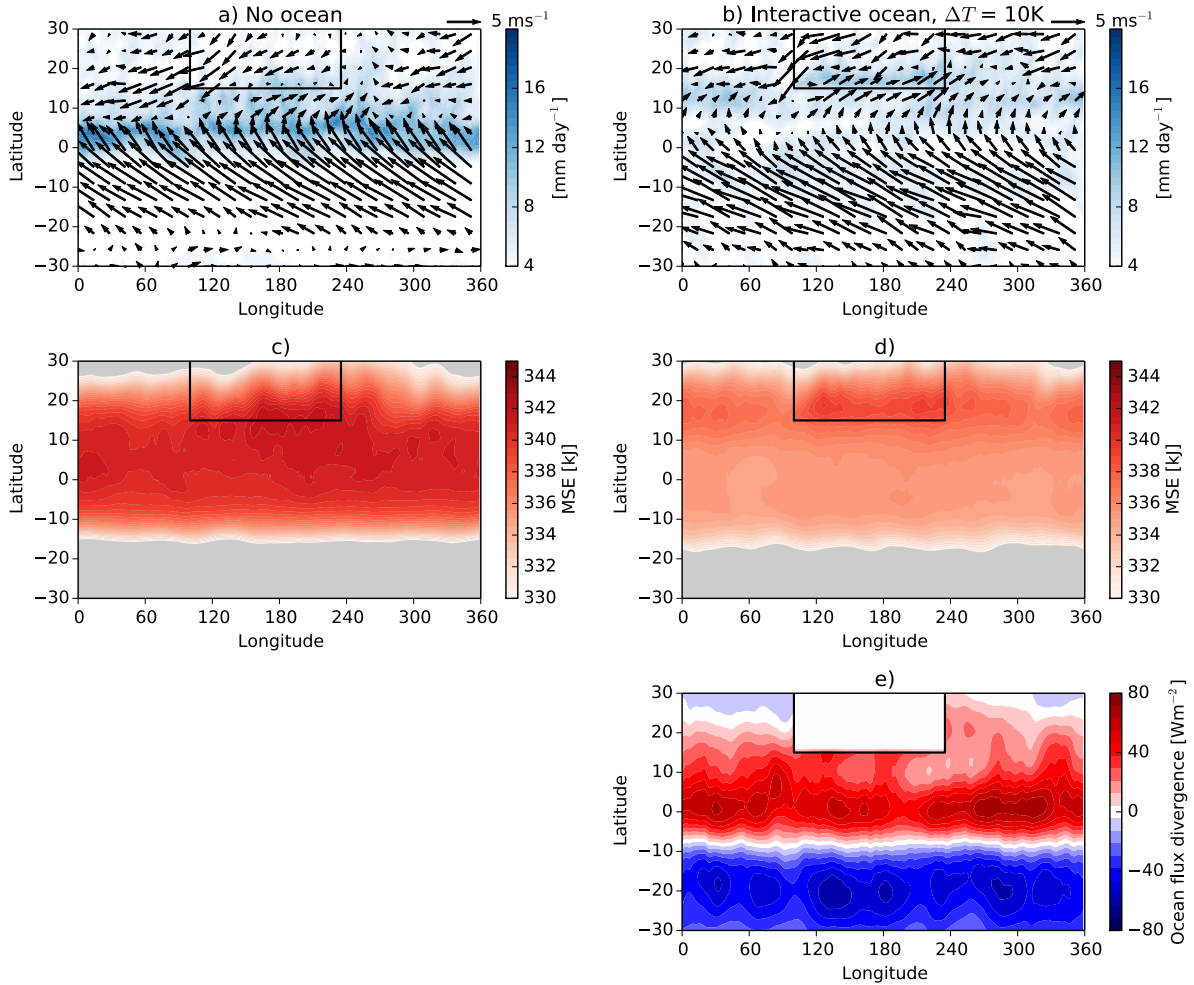
- 522 Walker, C. C., and T. Schneider, 2006: Eddy influences on hadley circulations: Simulations with  
523 an idealized gcm. *Journal of the Atmospheric Sciences*, **63 (15)**, 3333–3350.
- 524 Webster, P. J., C. Clark, G. Cherikova, J. Fasulla, W. Han, J. Loschnigg, and K. Sahami, 2002:  
525 The monsoon as a self-regulating coupled oceanatmosphere system. *International Geophysics*,  
526 **83 (2)**, 198–219.
- 527 Webster, P. J., and S. Yang, 1992: Monsoon and enso: Selectively interactive systems. *Quarterly*  
528 *Journal of the Royal Meteorological Society*, **118 (23)**, 877–926.
- 529 Zhai, J., and W. Boos, 2015: Regime transitions of cross-equatorial hadley circulations with zon-  
530 ally asymmetric thermal forcings. *Journal of the Atmospheric Sciences*, **64 (23)**, 3800–3818.



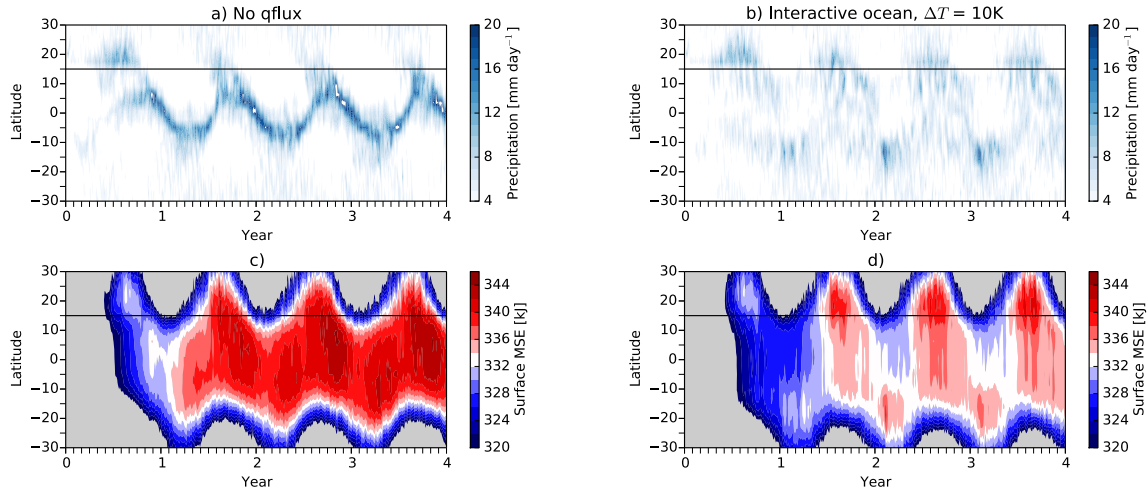
531 FIG. 1. Climatological June-July-August (JJA) downward energy flux at the ocean surface (contours) and  
 532 surface winds (arrows) from the NCEP reanalysis for the period 1979 to 2011.



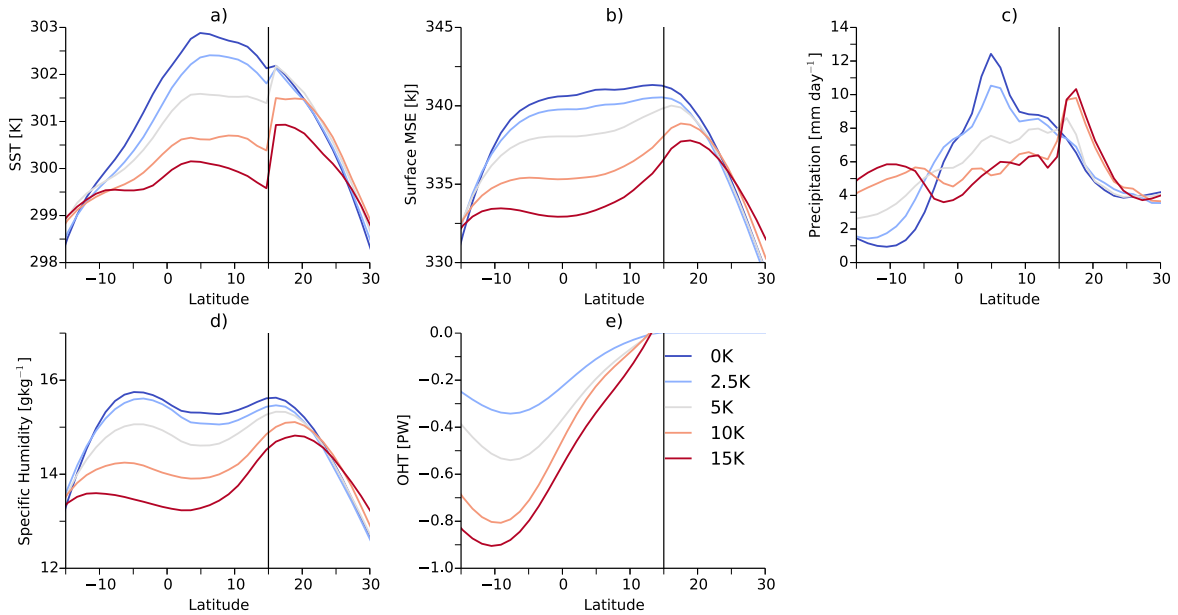
533 FIG. 2. Schematic of the model configuration used in the experiments. Note that the boundaries of the  
 534 interactive ocean move seasonally.



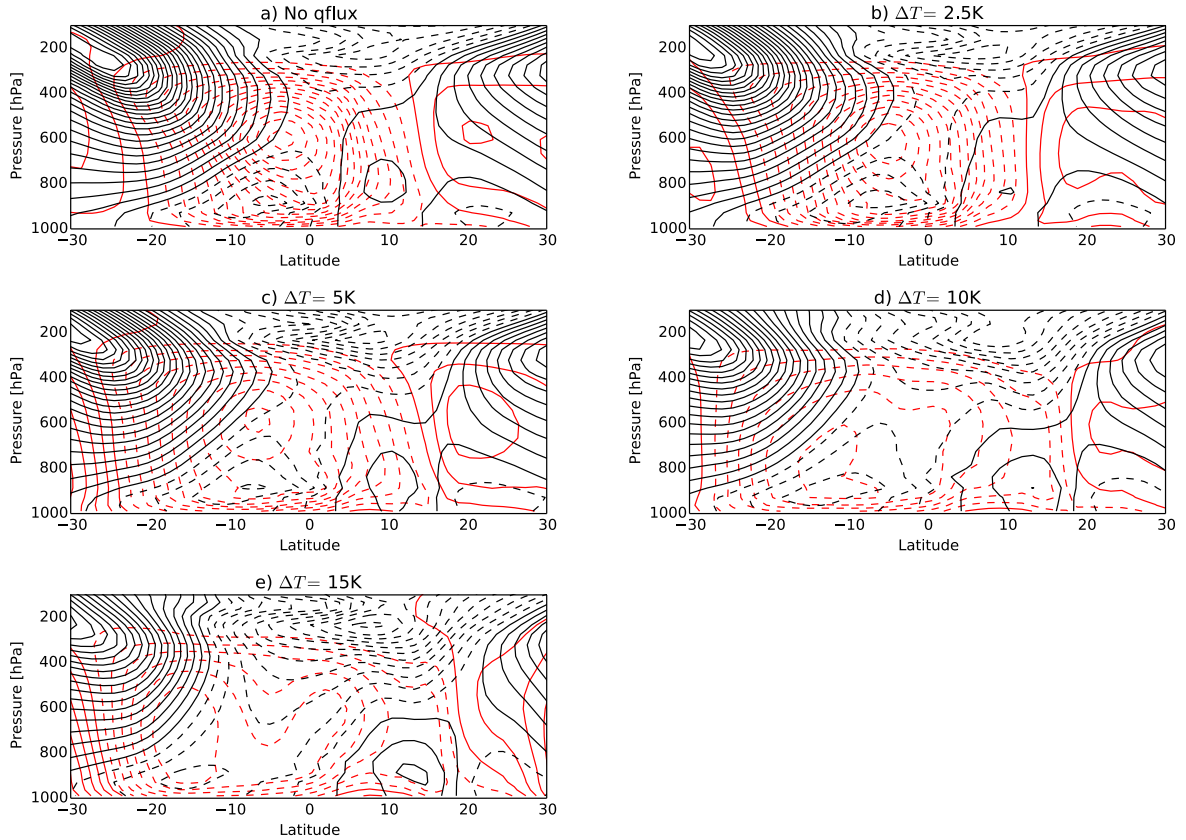
535 FIG. 3. a), b) Summer-time precipitation (blue contours) and winds at the lowest model level (arrows) for the  
 536 experiment with no OHT (a) and the experiment with interactive OHT and  $\Delta T = 10K$  (b). c), d) Moist static  
 537 energy (MSE) at the lowest model level from the same experiments. Gray regions have MSE values outside the  
 538 colorbar scale. e) OHT divergence from the experiment with interactive OHT.



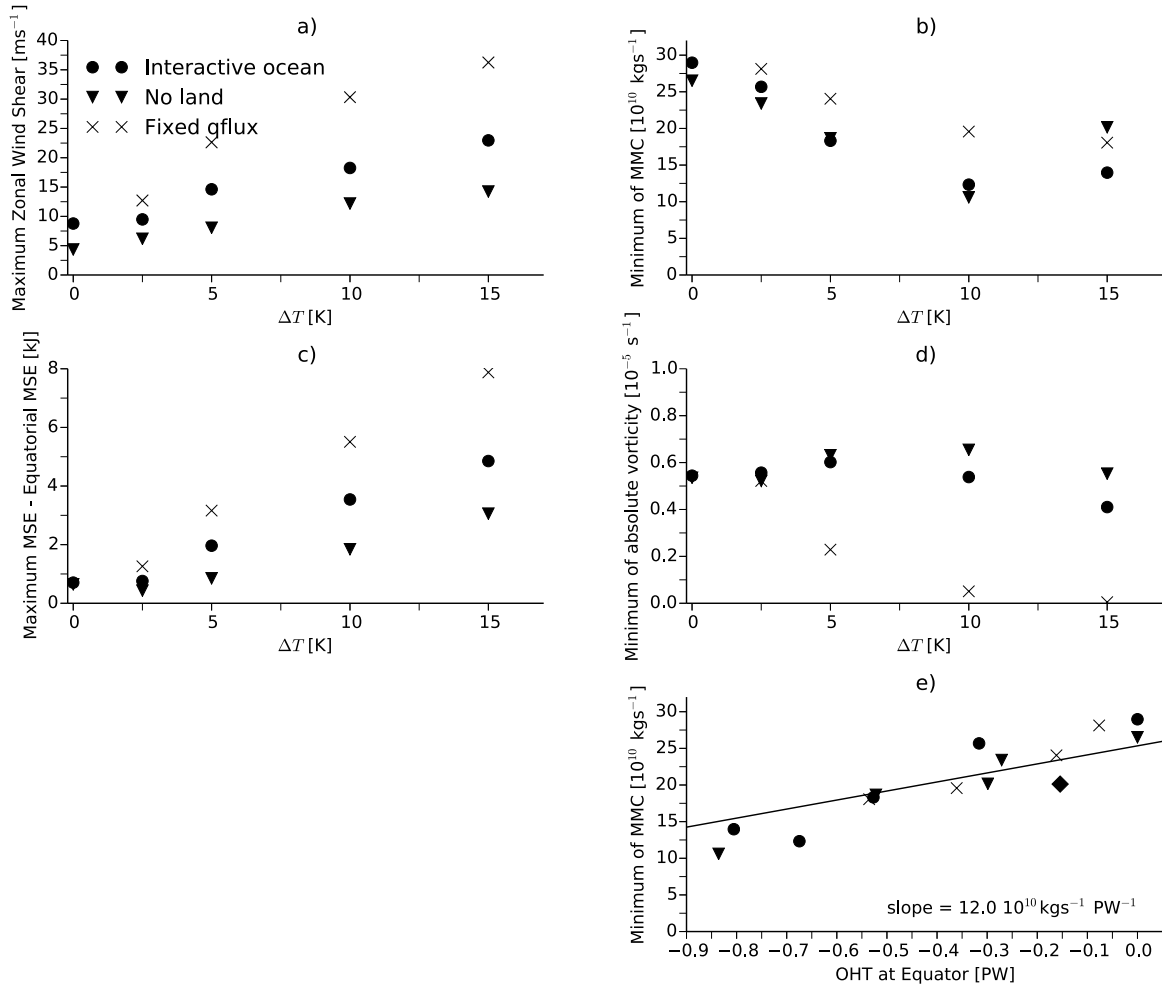
539 FIG. 4. a), c) Hovmuller diagrams of the precipitation (a) and surface MSE (c), averaged over  $100^{\circ}$  to  $235^{\circ}$ E,  
 540 for the land simulation with no OHT. b), d) Same for the land simulation with interactive OHT and  $\Delta T = 10$ K.  
 541 The horizontal black lines mark the southern edge of the continent. Note that the model is initialized at year 0.



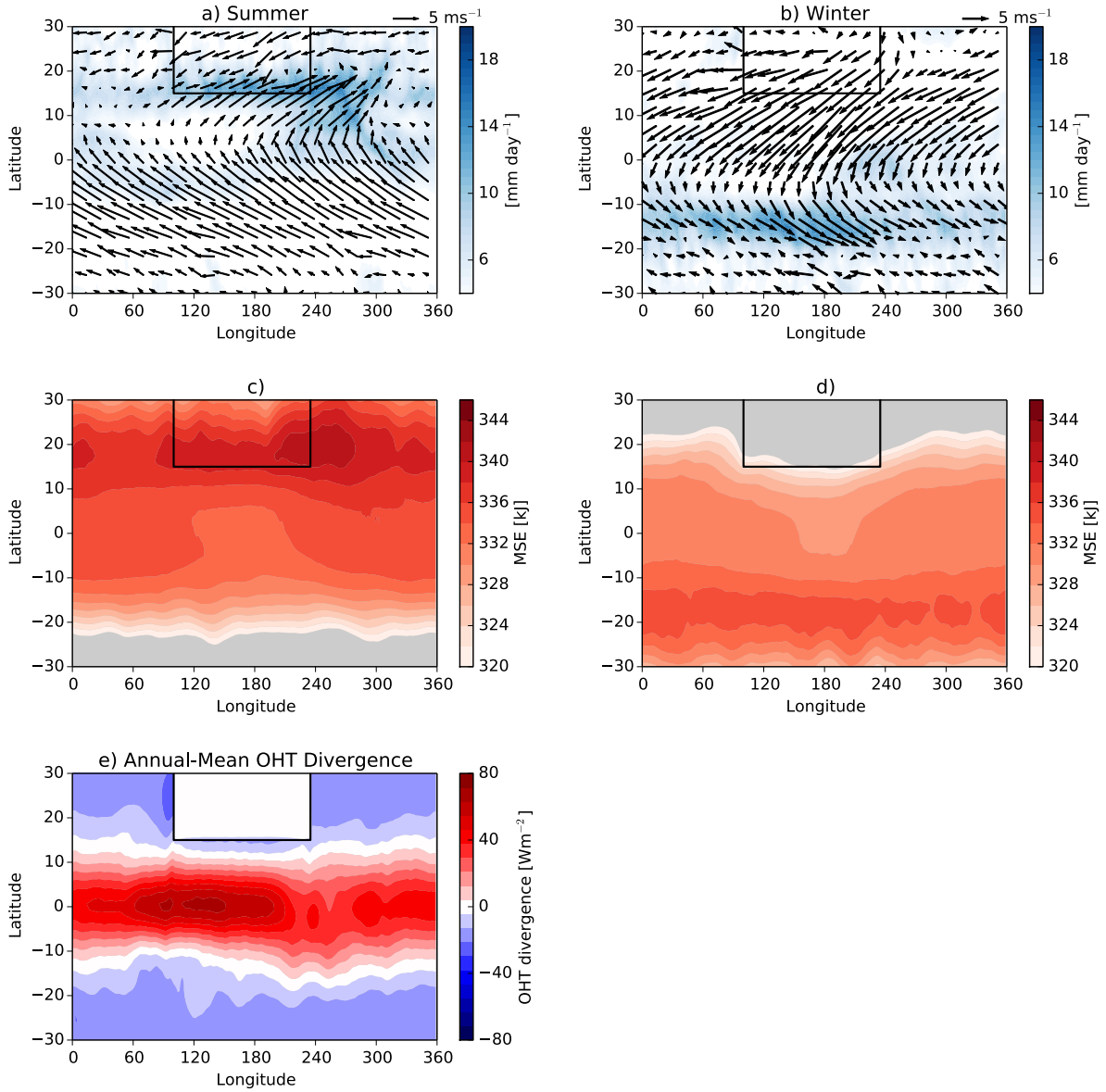
542 FIG. 5. a) Summer SSTs, averaged from  $100^{\circ}$  to  $235^{\circ}$ E, in the simulations with land and with  $\Delta T$  varied  
 543 from 0K to 15K. The vertical line marks the southern boundary of the continent. b) Averaged summer surface  
 544 MSE in these simulations. c) Averaged summer precipitation in these simulations. d) Averaged summer specific  
 545 humidity in these simulations. e) Averaged summer OHT in these simulations.



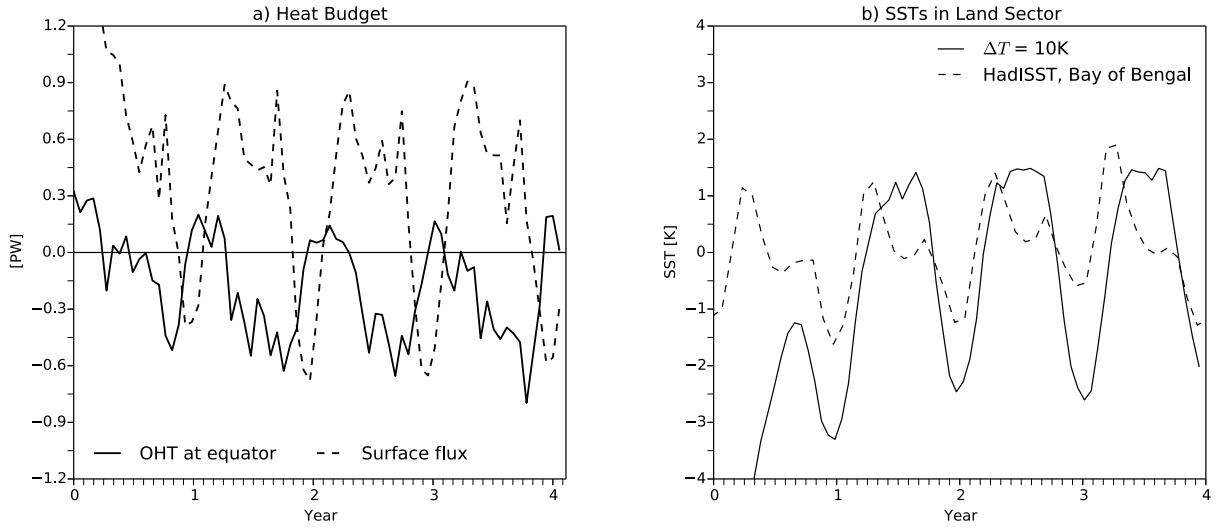
546 FIG. 6. a) Summertime mean meridional circulation (MMC, red contours) and zonal winds (black contours)  
 547 averaged over the land sector ( $100^{\circ}$  to  $235^{\circ}$ E) in the land simulation with  $\Delta T = 0$ K. The contour intervals are  $2$   
 548  $\times 10^9 \text{ kgs}^{-1}$  for the MMC and  $2 \text{ ms}^{-1}$  for the zonal wind. Dashed red contours denote counterclockwise circula-  
 549 tion and dashed black contours denote negative zonal wind speeds. b) Same for the simulation with  $\Delta T = 2.5$ K.  
 550 c) Same for the simulation with  $\Delta T = 5$ K. d) Same for the simulation with  $\Delta T = 10$ K. e) Same for the simulation  
 551 with  $\Delta T = 15$ K.



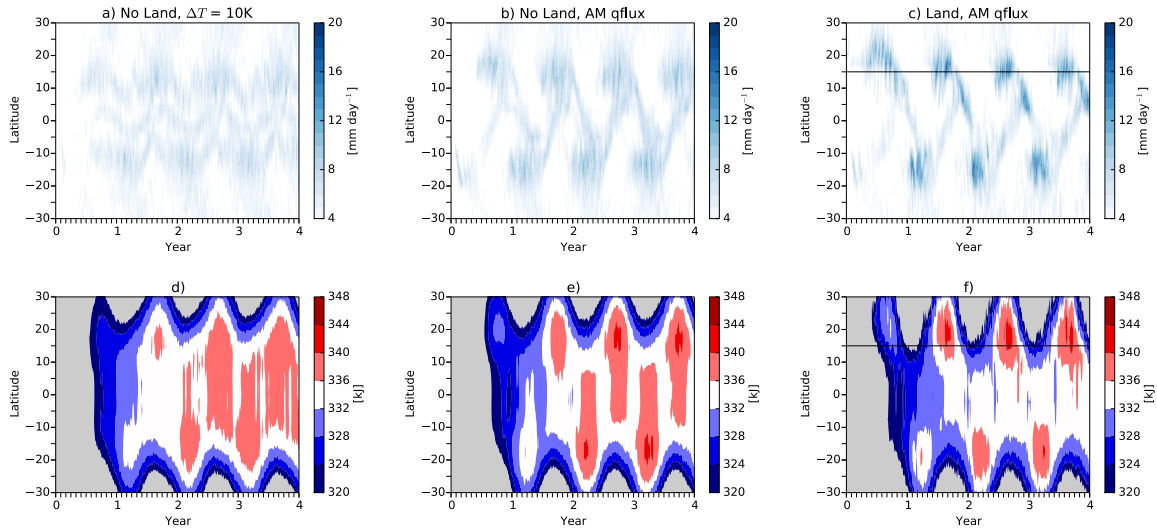
552 FIG. 7. a) Maximum of  $(u(850\text{hPa}) - u(250\text{hPa}))$ , averaged over the land sector ( $100^\circ$  to  $235^\circ\text{E}$ ), between  
 553 the equator and  $20^\circ\text{N}$  during the summer months for the simulations with land and interactive OHT (circles),  
 554 the simulations with interactive OHT and no land (triangles) and with land and OHT fixed at its annual-mean  
 555 values (crosses). b) Minimum of the summertime mean meridional circulation (MMC) for the same simulations.  
 556 c) Difference between maximum summer MSE and equatorial MSE at the equator for the same simulations. d)  
 557 Minimum absolute vorticity polewards of  $7^\circ\text{N}$  during the summer of the same simulations. e) Minimum of the  
 558 summertime MMC for the same simulations as a function of the equatorial OHT in the land sector. The line  
 559 shows a linear least-squares fit.



560 FIG. 8. a) Summer precipitation (contours) and near-surface winds (arrows) in the simulation with land and  
 561 OHT fixed at its annual-mean value from the  $\Delta T$  simulation with land. c) Summer near-surface MSE from the  
 562 same simulation. b), d) Winter precipitation and near-surface MSE from the same simulation. e) Annual-mean  
 563 OHT divergence in the  $\Delta T = 10\text{K}$  simulation with land.



564 FIG. 9. a) Ocean heat transport across the equator, integrated from  $100^{\circ}$  to  $235^{\circ}$ E (solid line) and net surface  
 565 flux integrated over the region  $100^{\circ}$  to  $235^{\circ}$ E and  $0^{\circ}$  to  $15^{\circ}$ N, from the land simulation with  $\Delta T = 10$ K (dashed  
 566 line). The heat transport is positive when it is northward. b) SSTs averaged over the region ( $100^{\circ}$  to  $235^{\circ}$ E and  
 567  $0^{\circ}$  to  $15^{\circ}$ N) from the simulation with  $\Delta T = 10$ K (solid line) and SSTs averaged over the Bay of Bengal ( $80^{\circ}$  to  
 568  $95^{\circ}$ E and  $0^{\circ}$  to  $15^{\circ}$ N) for the period 2012 to 2016, taken from the HadISST dataset.



569 FIG. 10. a), d) Hovmuller diagrams of zonal-mean precipitation (a) and meridional gradient of surface MSE  
 570 (d) for the simulation with no land and  $\Delta T = 10$ K. b), e) Same for the simulation without land and with OHT  
 571 fixed at its annual-mean value from the  $\Delta T = 10$ K simulation. c), f) Same for the simulation with land and with  
 572 OHT fixed at its annual-mean value from the  $\Delta T = 10$ K simulation.